Three Band Temperature Extraction from Airborne Imagery with Imprecise Atmospheric Knowledge

Carl Salvaggio[a], Marvin Boonmee[a], Natalie M. Sinisgalli[a], & David W. Messinger[a]

[a]Digital Imaging and Remote Sensing Laboratory
Chester F. Carlson Center for Imaging Science
Rochester Institute of Technology

ABSTRACT

The accurate estimation of surface object temperature from airborne imagery is complicated by several factors including the effects of the atmosphere, surface emissivity variations, and BRDF effects. Several methods have been proposed to handle specific cases where some of the unknowns can be eliminated. Typically, these methods use one or two spectral bands or viewing geometries and are applied to large, homogeneous surfaces where the surface emissivity can be approximated as a black body. In particular, a method using two spectral bands for sea-surface temperature estimation with the AVHRR sensor has shown success while removing the need for an estimate of the atmospheric upwelling radiance. Here, this method is extended to include a third band measurement and is applied to terrestrial targets. The algorithm has been tested against a synthetic scene containing a wide variety of targets. Temperature prediction capabilities are modestly improved by inclusion of the third radiance band measurement. Sensitivity studies demonstrate that the inclusion of the third band slightly decreases the sensitivity of the algorithm to knowledge of the atmospheric transmission and downwelling radiance. This is true even for stressing cases such as hot targets and targets with very low emissivity. It is also shown that for both methods precise knowledge of the downwelling radiance is the least significant input parameter for accurate surface temperature estimation.

Keywords: LWIR, Temperature Estimation, Split Window Technique, DIRSIG

1. INTRODUCTION

The development of airborne and space-based thermal infrared sensors has provided researchers the ability to monitor targets of interest based not only on reflected solar radiation but also on the thermal emission due to the objects themselves. This measured emission has a spectral "shape" that is determined by both the Planck blackbody radiance curve and the spectral emissivity of the target (assuming the target is not a blackbody). If the object were observed directly with minimal (or no) intervening atmospheric effects, estimation of the object temperature given knowledge of the material emissivity is a straightforward process. However, the presence of the atmosphere adds a significant source of confusion to the process of inverting the measured at-sensor radiance to the surface target temperature. Surface-emitted photons can be either absorbed or scattered by the atmosphere, or the atmosphere can emit or scatter photons into the line of sight. The atmospheric contributions are termed here the *upwelling radiance*, or that radiance emitted / scattered by the atmosphere into the line of sight, the *downwelling radiance*, or that radiance emitted / scattered by the atmosphere onto the target, and the *atmospheric transmission*. These three properties of the atmosphere must be measured or estimated to remove their effects from the temperature estimation problem.

Methods exist to estimate the contributions to the at-sensor radiance from the atmosphere,[1] and in an ideal case, a co-located and co-temporal radiosonde measurement of the atmospheric constituents can be combined with a model-based approach to predict the atmospheric contributions. Predictive models such as MODTRAN[2, 3] are commonly used for just such a purpose. However, any errors or uncertainties in the predictive model limit the accuracy with which the atmospheric contributions can be estimated, thus impacting the ability to estimate the surface temperature. Alternatively, direct measurements of these properties can be attempted. However, this

Further information: Chester F. Carlson Center for Imaging Science, Rochester Institute of Technology, 54 Lomb Memorial Dr., Rochester, NY 14623, salvaggio@cis.rit.edu

typically requires ground-based instruments at the site of interest. Also, accurate measurement of the downwelling radiance is difficult as one must account for contributions from the entire visible sky dome. Methods to determine the atmospheric contribution based solely on in-scene properties are also available. The In-Scene Atmospheric Compensation algorithm[4] (ISAC) is commonly used with hyperspectral longwave Infrared data. Here, it is assumed that a significant portion of the image is nearly a blackbody, and that the atmosphere is relatively constant over the entire image. The Autonomous Atmospheric Compensation algorithm[5] (AAC) combines in-scene and model-based methods to produce estimates of the atmospheric contributions to the measured radiance. Here, statistical correlations between scene-derived parameters and MODTRAN model predictions are developed and used to determine the atmospheric transmission and upwelling and downwelling radiances.

Algorithms for the estimation of surface temperature using observations from multiple angles[1, 6, 7] have been developed and applied to satellite-based measurements with good results under appropriate circumstances. The Multiple Angle Method utilizes the differential absorption due to different atmospheric pathlengths for a common target. However, this method relies on the assumptions that the atmospheric column is spatially uniform over the entire scene of interest, the observations must have a significant path difference, and that the directional emissivity effects of the targets are either negligible or well-known. Alternatively, methods using predictive radiative transfer models have also been developed and used.[1] These can rely on the combination of an atmospheric model with a radiosonde (or satellite sounding) of the area of interest. These methods can be particularly good for validating other methods or for establishing statistical coefficients for a parameterized approach. Other methods include single channel techniques[8] and the Temperature Emissivity Separation algorithm.[9]

Of particular interest here is the Split Window Technique (SWT) as described by Prata (1993). This method was originally developed to estimate Sea Surface Temperature[10–15] and later adapted to Land Surface Temperature (LST) with the Advanced Very High Resolution Radiometer (AVHRR) channels 4 (10.8 μm) & 5 (11.9 μm). By combining information from two spectral bands, a method was developed that does not require knowledge of the atmospheric upwelling radiance. The method works particularly well for flat terrain with a uniform surface composition of known emissivity. Prata (1993) develops the two band method in some detail and examines the sensitivities of the method to effects such as the target emissivity characteristics and the dependence on zenith angle. The method is described as being particularly sensitive to accurate estimation of the surface emissivity and the assumption of a Lambertian surface.

This paper describes an extension of the Split Window Technique of Prata (1993) to use of a third spectral channel. The third channel is used to derive an improved estimate of the Planck radiance in the "second" channel. Theoretically, the addition of more information should improve the temperature estimation accuracy. Several combinations of spectral channels spanning the Midwave Infrared (MWIR, 3-5 μm) and the Longwave Infrared (LWIR, 8-14 μm) are used and their estimation accuracy are determined through the use of synthetic imagery.

This paper is organized in the following way. Section 2 describes both the original two-band SWT as well as the extension to a third band of information. Here, an error analysis of assumptions made in the derivation is also provided. Section 3 describes the data used to test the algorithm while Section 4 presents the results of the experimentation. Section 5 provides a summary of the work and conclusions.

2. ALGORITHM DESCRIPTION

The two-band Split Window Technique (SWT) as developed by Prata (1993) assumes a Lambertian surface with a temperature close to the temperature of the lower layer of the atmosphere. As applied to the AVHRR sensor, with a pixel spatial resolution of approximately one kilometer, the algorithm also assumes a uniform surface emissivity close to one over the pixel of interest. The two-band method is derived here for completeness with the extension to a third band provided after.

2.1. Two-Band Split Window Technique

As stated above, the two-band SWT has been applied to AVHRR channels 4 (10.8 μm) & 5 (11.9 μm) with good results over large, uniform, near-blackbody targets of interest. We start by writing the at-sensor radiance as

$$L_i = \left[\epsilon_i B_i(T_s) + (1-\epsilon_i) L_{d,i}\right] \tau_i + L_{u,i} \tag{1}$$

where L_i is the measured radiance in band i, ϵ_i is the surface emissivity in that band, $B_i(T)$ is the Planck blackbody radiance in band i due to a blackbody at temperature T, T_s is the surface temperature, $L_{d,i}$ is the atmospheric downwelling radiance, τ_i is the atmospheric transmission, and $L_{u,i}$ is the atmospheric upwelling radiance. The first term thus represents the surface emitted radiance, the second term represents skylight reflected by the surface (assuming the surface is opaque and the reflectance can be written as $(1-\epsilon_i)$), and both of these are attenuated by the atmosphere. We can approximate the sky upwelling radiance as coming from a modified blackbody at an effective temperature,

$$L_{u,i} = (1-\tau_i)\, B_i\left(\bar{T}_a\right). \tag{2}$$

Here, we approximate the effective emissivity of the atmosphere as $(1-\tau_i)$.

Now, the radiances in bands 1 & 2* can be written as

$$\begin{aligned} L_1 &= \left[\epsilon_1 B_1(T_s) + (1-\epsilon_1) L_{d,1}\right]\tau_1 + (1-\tau_1)\, B_1\left(\bar{T}_a\right) \\ L_2 &= \left[\epsilon_2 B_2(T_s) + (1-\epsilon_2) L_{d,2}\right]\tau_2 + (1-\tau_2)\, B_2\left(\bar{T}_a\right) \end{aligned} \tag{3}$$

where the subscripts refer to the particular band of interest. If we assume that bands 1 & 2 are spectrally close to each other, the Planck radiation in band 2 can be approximated using a truncated Taylor series expansion of the Planck equation around band 1:

$$B_2(T) \approx B_1(T) + \Delta\lambda \frac{\partial B_1}{\partial \lambda} \tag{4}$$

with $\Delta\lambda = \lambda_2 - \lambda_1$. Using this approximation we can write the radiance in band 2 that has the same brightness temperature as the inverse Planck function when evaluated at band 1 as

$$\begin{aligned} L_1' &\approx \epsilon_2\tau_2 B_2(T_s) + (1-\tau_2)\, B_1(\bar{T}_a) + (1-\epsilon_2)\, L_{d,2}\tau_2 \\ &+ \epsilon_2\tau_2\Delta\lambda\left(\frac{\partial B_1(T_s)}{\partial\lambda} - \frac{1}{\epsilon}\frac{\partial B_1(\bar{T}_a)}{\partial\lambda}\right) \\ &+ \Delta\lambda\left(\frac{\partial B_1(\bar{T}_a)}{\partial\lambda} - \frac{\partial B_1(T_{b,2})}{\partial\lambda}\right). \end{aligned} \tag{5}$$

The last two terms involving the derivatives of the Planck function are assumed small due to the nature of the Planck function at different temperatures and are neglected. An investigation into the impact of this assumption is presented below in Section 2.3. This expression now can be equated with L_1 in Equation 3 and the Planck radiance in band 1 due to the surface temperature can be isolated as

$$\begin{aligned} B_1(T_s) &= \frac{(1-\tau_2)L_1}{(1-\tau_2)\epsilon_1\tau_1 - (1-\tau_1)\epsilon_2\tau_2} \\ &- \frac{(1-\tau_1)L_1'}{(1-\tau_2)\epsilon_1\tau_1 - (1-\tau_1)\epsilon_2\tau_2} \\ &+ \frac{(1-\tau_1)(1-\epsilon_2)\tau_2 L_{d,2} - (1-\tau_2)(1-\epsilon_1)\tau_1 L_{d,1}}{(1-\tau_2)\epsilon_1\tau_1 - (1-\tau_1)\epsilon_2\tau_2}. \end{aligned} \tag{6}$$

This can be inverted directly to the surface temperature if we approximate L_1' as

$$L_1' \approx B_1(T_{b,2}), \tag{7}$$

where $T_{b,2}$ is the brightness temperature in band 2.

In summary, given estimates of the atmospheric transmission and downwelling radiance in the two chosen bands, as well as an estimate of the surface emissivity in those bands, the surface temperature can be estimated from the Planck radiation of the surface in band 1 given by Equation 6. By using this combination of the two bands, knowledge of the atmospheric upwelling radiance is not required.

*Throughout this paper we refer to bands 1, 2, & 3 as the channels of interest to the method. As this is being developed without a particular sensor in mind, we are avoiding the notation of Prata (1993) which refers specifically to AVHRR bands 4 & 5.

2.2. Three-Band Split Window Technique

While the two-band technique does provide a reasonable method for Land Surface Temperature (LST) estimation, it may be possible to improve the estimation accuracy or decrease the dependence on the atmospheric contributions through the addition of a third measured spectral radiance. Now, similar to Equation 3 we write

$$\begin{aligned} L_1 &= [\epsilon_1 B_1(T_s) + (1-\epsilon_1)L_{d,1}]\,\tau_1 + (1-\tau_1)\,B_1\left(\bar{T}_a\right) \\ L_2 &= [\epsilon_2 B_2(T_s) + (1-\epsilon_2)L_{d,2}]\,\tau_2 + (1-\tau_2)\,B_2\left(\bar{T}_a\right) \\ L_3 &= [\epsilon_3 B_3(T_s) + (1-\epsilon_3)L_{d,3}]\,\tau_3 + (1-\tau_3)\,B_3\left(\bar{T}_a\right) \end{aligned} \tag{8}$$

where quantities with subscript 3 refer to the third band. Here, bands 1, 2, & 3 will be treated as being of sequentially longer wavelength, although this is not necessarily required.

Essentially, the three-band extension is an iteration of the above-described two-band method. In words, bands 2 & 3 are used to derive an estimate for the band 2 Planck radiance, $\hat{B}_2(T_s)$, as in Equation 6 (with 2 replaced by 3 and 1 replaced by 2). This estimate is used instead of the Taylor series expansion as done in the two-band method. Now, the band 2 radiance can be written as

$$L_2 \approx \epsilon_2\tau_2\hat{B}_2(T_s) + (1-\epsilon_2)\tau_2 L_{d,2} + (1-\tau_2)B_2(\bar{T}_a). \tag{9}$$

Where before, the Planck function in band 2 was expanded using a Taylor series in terms of the Planck function in band 1, here it is estimated from the band 3 information and used directly.

Now, with expressions for both L_1 and L_2, each can be solved for $B_1(\bar{T}_a)$ (with the term for $B_1(\bar{T}_a)$ in L_2 coming from the Taylor series expansion) and equated. This expression is then solved for the term that is dependent only on the surface temperature, $B_1(T_s)$, to give

$$\begin{aligned} \frac{(1-\tau_2)\epsilon_1\tau_1 B_1(T_s)}{(1-\tau_1)} &= \frac{(1-\tau_2)L_1 - (1-\tau_2)(1-\epsilon_1)\tau_1 L_{d,1}}{(1-\tau_1)} \\ &- L_2 + \epsilon_2\tau_2\hat{B}_2(T_s) \\ &+ (1-\epsilon_2)L_{d,2}\tau_2 \\ &+ \Delta\lambda\left[(1-\tau_2)\left(\frac{\partial B_1(\bar{T}_a)}{\partial\lambda}\right) - \left(\frac{\partial B_1(T_s)}{\partial\lambda}\right)\right]. \end{aligned} \tag{10}$$

Again, the last term involving the partial derivatives of the Planck function is ignored in the surface temperature estimation. The Planck radiance in band 1 can be solved for and inverted to the surface temperature.

2.3. Error Analysis of Neglected Terms

In the derivation of both the two-band and three-band split window techniques, terms involving the derivatives of the Planck function were ignored in the final estimation of the surface temperature. As can be seen in Equation 5, for targets of high emissivity, and for conditions where the effective atmospheric temperature is near the surface temperature, these terms are negligible. Even for a significant difference in these temperatures, the spectral nature of the Planck function ensures that, as long as the measurements are not near to, and on the same side of, the peak in the blackbody radiance curve, these derivatives must be very similar (assuming a relatively smooth spectral emissivity).

For this work, where the surface emissivity is not assumed to be close to one, a numerical analysis of the magnitude of these terms was conducted. Results of this experiment are shown in Figure 1. Here, the magnitude of the combination of those terms, in radiance units, is shown as a function of the actual surface temperature for a number of emissivities and two atmospheric conditions. The curves are iso-emissivity curves ranging from $\epsilon = 1.0$ (nearest radiance equal to zero) to $\epsilon = 0.2$ (furthest from zero) in increments of $\epsilon = 0.05$. Figure 1 (a) is for the MODTRAN Sub-artcic Winter atmosphere and (b) is for the MODTRAN Tropical atmosphere (chosen to represent very low water vapor concentration and very high water vapor concentration cases). Here, the brightness temperature in the second band, $T_{b,2}$ and the effective atmospheric temperature, $\bar{T}_a$, were set to 265 K and the atmospheric transmittance was set to 0.94. The wavelengths for the calculation corresponded to

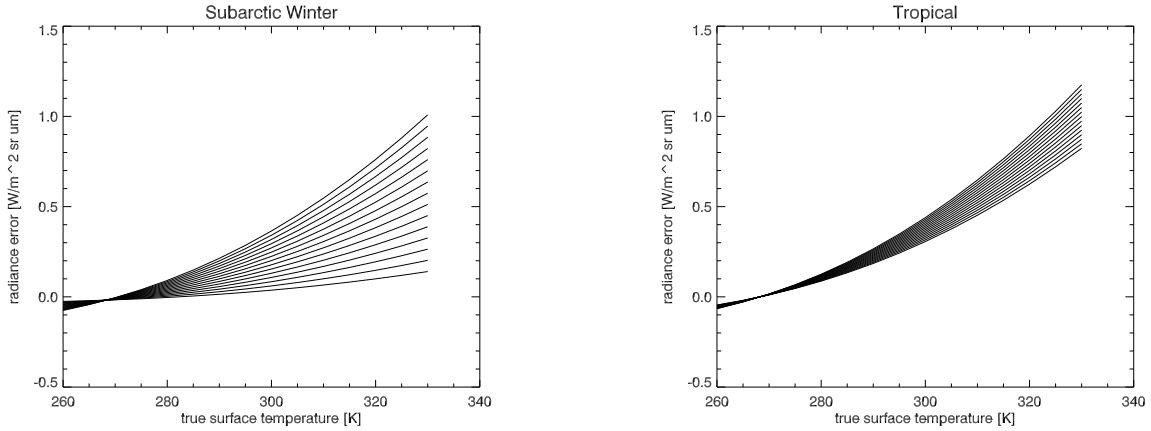

(a) **(b)**

Figure 1. Error analysis as a function of true surface temperature for the neglected terms for the two-band derivation in Equation 5. Curves are iso-emissivity curves running from $\epsilon = 1.0$ (nearest to zero radiance) to $\epsilon = 0.2$ (furthest from zero). (a) MODTRAN Sub-arctic Winter atmosphere. (b) MODTRAN Tropical atmosphere.

bands 4 & 5 of the AVHRR sensor. Note that the Planck radiance for a blackbody at $\lambda = 11\ \mu$m, near the wavelengths of interest here, is approximately 10 [W/(m^2 sr μm)] - roughly an order of magnitude greater than the most extreme error made in ignoring these terms. Consequently, the terms involving the Planck function derivatives will be ignored for the remainder of this work.

It is worth noting, however, that the method is generally worse for the Tropical atmosphere (greater water vapor concentration). Also, note that for emissivities that deviate far from blackbody, the error is significantly worse than for near-blackbody targets. This is particularly true for the relatively dry, Sub-arctic winter atmosphere. This result agrees with Prata (1993) where a relatively dry atmosphere is cited as a required condition for application of the Split Window Technique.

Both the two-band and three-band Split Window Techniques for temperature estimation were implemented in IDL / ENVI for testing. Required inputs to the tool are (1) a radiance image of the scene, (2) regions of interest for which the temperature is to be estimated (assuming several pixels on target), (3) estimates of the atmospheric contributions (L_d & τ) for the scene for each spectral band, and (4) estimates of the target emissivity (ϵ) for each spectral band and region of interest. The tool returns the estimated surface temperature minimum, mean, maximum, and standard deviation over the region of interest selected.

3. TEST DATA

The three-band extension to the Split Window Technique was not developed with a particular sensor in mind. Consequently, the method was tested against high-fidelity synthetic imagery simulating a multispectral sensor with several bands over the MWIR and LWIR spectral regions. The synthetic scene was created using DIRSIG, the **D**igital **I**maging and **R**emote **S**ensing **I**mage **G**eneration tool developed at RIT. DIRSIG is a physics-based, first-principles ray tracing simulation incorporating full three-dimensional object geometry coupled with field and laboratory measurements of material physical and optical properties.[16,17] Atmospheric effects are modeled using MODTRAN[2,3] and the scene can be spatially and spectrally oversampled providing accurately mixed pixels. A temperature prediction model estimates the temperature of every facet in the scene based on material thermodynamic and optical properties, illumination history, and local weather history.

The scene to be used here is of a terrestrial target - a water treatment plant based on an area of Northeast Rochester, NY. A black and white version of a visible rendering is shown in Figure 2. Targets of interest in the

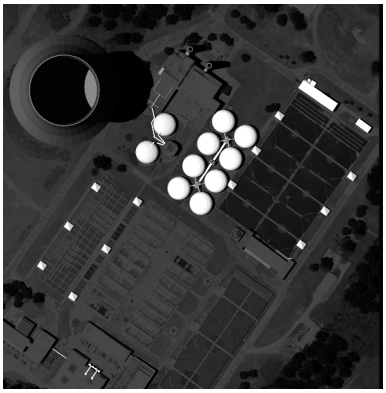

Figure 2. Visible rendering of the scene used in analysis for this study. Scene is of a water treatment plant with a cooling tower added.

scene include metallic tanks (one of which is the "control" target with a temperature of 278 K and an emissivity greater than 0.9), parking lots, large tanks with an emissivity artificially set to 0.4 (to test the algorithm sensitivity to L_d), and a tank with the temperature artificially set to 415 K (to test the algorithm performance against hot targets). The atmosphere was modeled as the standard MODTRAN Mid-Latitude Summer atmosphere. The GSD of the rendered scene is approximately one meter providing many pixels on the targets of interest. The scene was rendered using a fictional sensor at altitudes of 1,000 m and 10,000 m and a spectral response composed of seventeen spectral channels. Four spectral channels in the MWIR ranged from 3.5 to 5 μm, with centers every 0.5 μm. Similarly, there were twelve channels in the LWIR ranging from 8 to 14 μm, also spaced evenly at 0.5 μm increments. Additionally, as a more directly applicable test, the scene was rendered using the MODIS spectral response but with a fictional focal length to provide several pixels on the targets of interest.

4. RESULTS

4.1. Two-band & Three-band Estimation Comparison

Absolute errors from application of the two-band and three-band algorithms for the scene at 1km altitude are shown Figures 3 (a) & (b), respectively. Results for the 10km altitude scene are shown in Figure 4. For this experiment, the scene rendered with the "fictional" spectral response was used and band combinations were "sequential" (*e.g.*, band 1 = 9.0 μm, band 2 = 9.5 μm, & band 3 = 10.0 μm). In general, for both algorithms and for both altitudes the performance when using bands from the MWIR is worse than when using data from the LWIR, although the three band method performs better in the MWIR than the two band method. For the image rendered with a sensor altitude of 1 km (Figure 3), the three band algorithm performs better than the two band algorithm. The errors are smaller and less sensitive to the target of interest. In particular, the two band algorithm performs poorly against the low emissivity target while the three band algorithm produces reasonable temperature estimates for this target. Similar results are seen for the image with a sensor altitude of 10km (Figure 4). Here, however, the three band algorithm tends to overestimate the target temperature while at 1km altitude, the errors were generally negative. Again, the two band algorithm performs poorly for the low emissivity target with a wide range of temperature prediction errors.

4.2. Sensitivity Analysis

The sensitivity of the two-band and three-band algorithms was tested against the scene rendered using the MODIS configuration (rendered with the MODIS spectral response but artificially high spatial resolution). Band combinations were chosen such that performance was optimized for each algorithm. For the two-band algorithm, MODIS bands 31 & 32 were used. For the three band algorithm against the control and low emissivity targets,

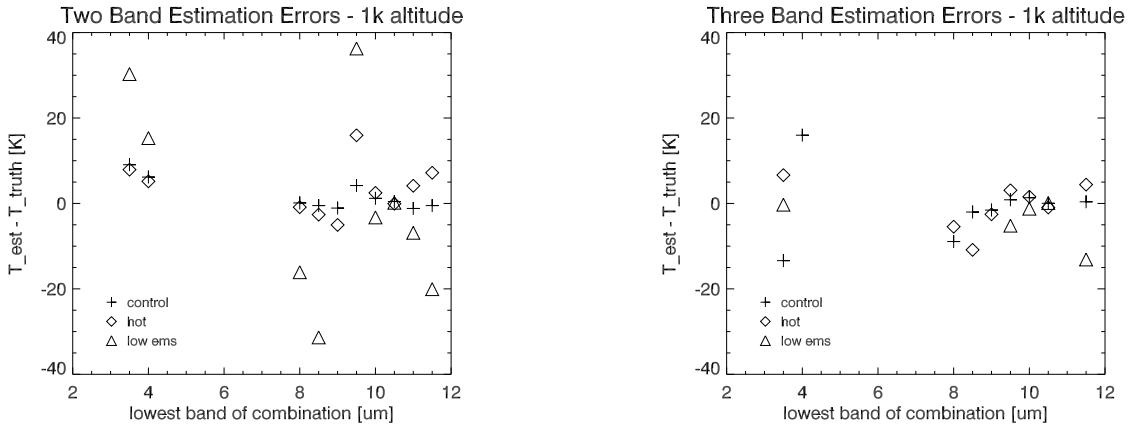

(a) **(b)**

Figure 3. Temperature estimation errors for (a) the two-band method and (b) the three-band method, both for the scene with sensor altitude of 1km. Symbols are for the control target, the hot target, and the low emissivity targets. The x-axis represents the lowest band in the (sequential) combination. Note that some errors are outside the plot range and not shown.

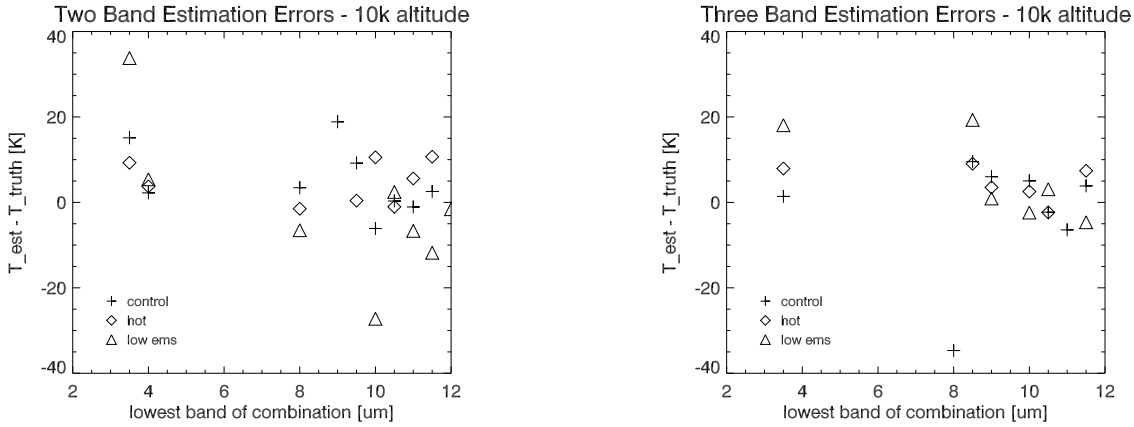

(a) **(b)**

Figure 4. Same as for Figure 3 but for the 10km altitude data.

MODIS bands 29, 30, & 32 were used. For the three band algorithm against the hot target, MODIS bands 30, 31, & 33 were used. Sensitivity to three parameters was tested: atmospheric transmission (τ), atmospheric downwelling radiance (L_d), and the target emissivity (ϵ). These quantities are all required for both methods. Here, the input values were deviated from 35% below to 15% above the truth values (but constrained to be physically viable, *i.e.*, emissivity and transmission can not be greater than one, L_d can not be negative).

The sensitivity of the two band and three band methods to the target emissivity is shown in Figure 5. Here we

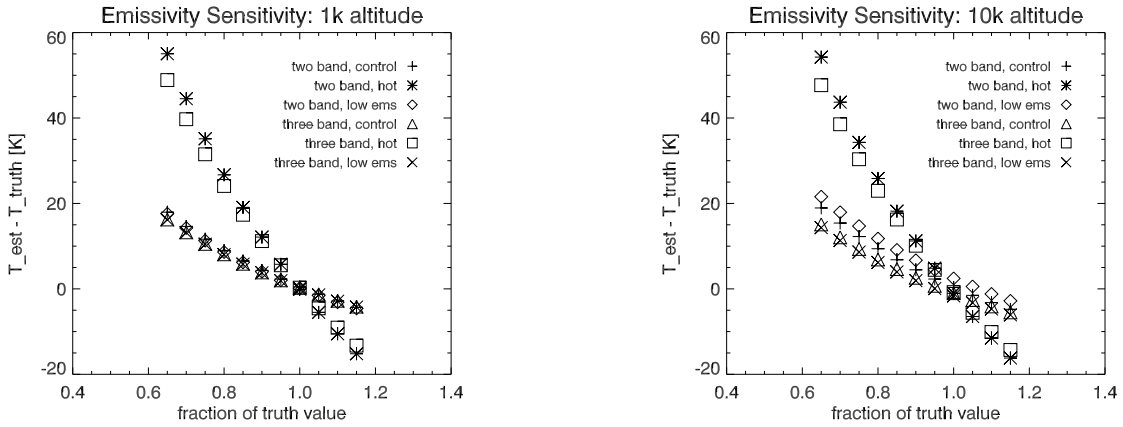

(a) **(b)**

Figure 5. Sensitivity of the algorithms to target emissivity knowledge.

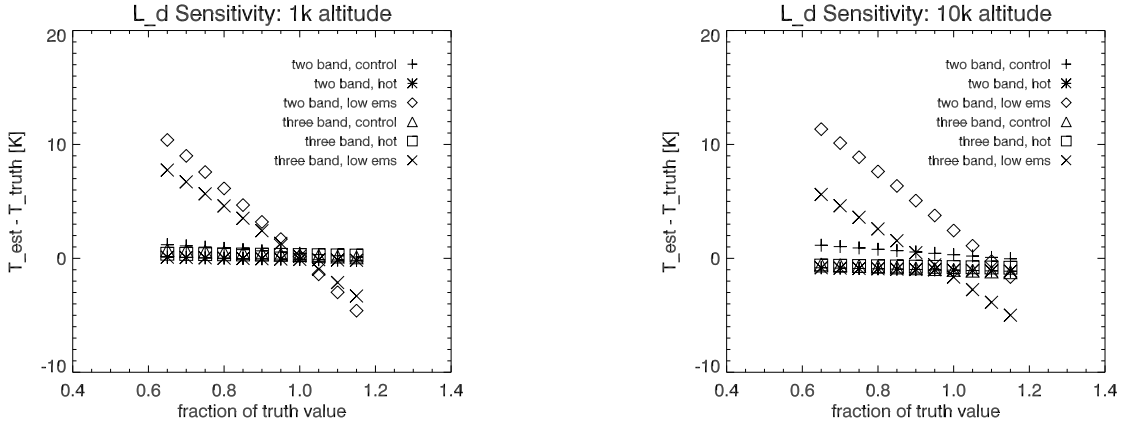

(a) **(b)**

Figure 6. Sensitivity of the algorithms to L_d knowledge. Note the scale change in the temperature error.

see that at both altitudes, the three band method is slightly less sensitive to knowledge of the surface emissivity than the two band method for the hot target. For most other targets, the performance is comparable between the two methods. In all cases, errors greater than $\approx 10\%$ result in temperature estimation errors of greater than 5 K. Figure 6 shows the sensitivity of the algorithms to knowledge of the downwelling radiance (L_d). For the 1km altitude the three band method gives lower errors than the two band method. The same is true for the 10km altitude except for overestimation errors in L_d. Note that, as expected, for targets other than those with low emissivity (here $\epsilon = 0.4$), both methods are relatively insensitive to knowledge of the downwelling radiance. As much as a 35% error can be made in the estimate of this parameter with as little as a 1-2 K error in the estimated temperature. Knowledge of this input parameter for high-emissivity targets does not impact the ability

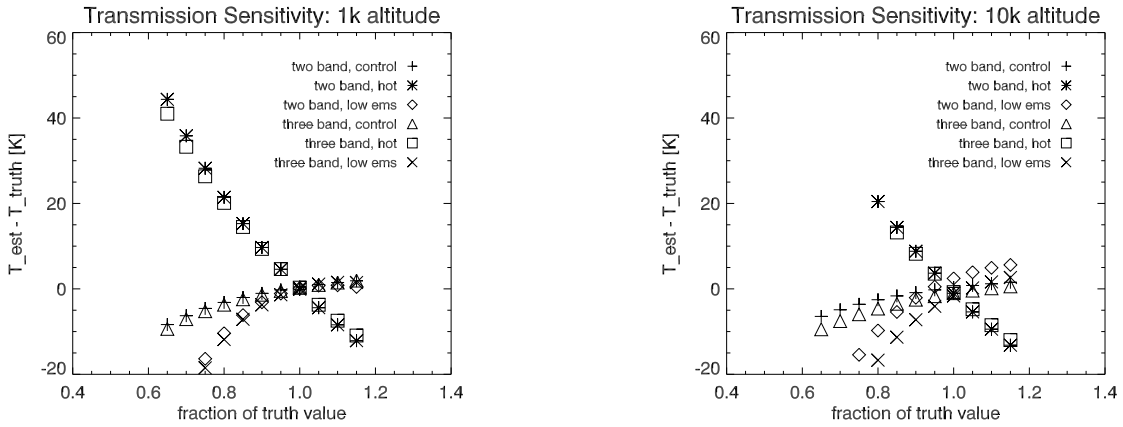

(a) **(b)**

Figure 7. Sensitivity of the algorithms to atmospheric transmission knowledge.

to predict the surface temperature. Figure 7 shows the algorithm sensitivity to knowledge of the atmospheric transmission. Here, there is no significant difference between the two band and three band methods.

Note, however, that for both the sensitivity to target emissivity and atmospheric transmission, both methods are particularly sensitive when estimating the temperature of hot targets in the scene. This is possibly due to a common set of bands being used for the analysis in each separate experiment. Due to the shift in the peak of the blackbody curve, it is highly likely that a band combination that performs well for a cooler target will not perform well for a hot target. The optimal band combination for each target was not sought in this research.

5. SUMMARY AND CONCLUSIONS

An extension to the two band Split Window Technique has been developed to include measured information from a third spectral channel. Both the two band and three band SWT algorithms were tested against synthetic scenes at two sensor altitudes including terrestrial targets of interest. Spectral coverage for the images included both the MWIR and the LWIR, and band combinations from both spectral regimes were tested. A control target with a temperature of 278 K was included, as well as a particularly hot target (415 K) and a target with low spectral emissivity ($\epsilon = 0.4$).

In general, the three band method performs slightly better than the two band method in terms of temperature prediction accuracy, particularly for the low emissivity target and when MWIR bands are used in the analysis. Also, the three band method is less sensitive than the two band method to the required input parameters. It is also shown that, except for the low emissivity target, both methods are insensitive to knowledge of the atmospheric downwelling radiance. Given limited resources, accurate estimation of this parameter should be given lower relative priority than the atmospheric transmission or target emissivity. These results indicate that modest improvements may be achieved with the addition of a third measured radiance, but the creation of a three band sensor may not be justifiable if a two band sensor is readily available.

ACKNOWLEDGMENTS

The authors would like to thank Mr. David Pogorzala for his assistance in simulation of the test scene used.

REFERENCES

1. P. Dash, F.-M. Göttsche, F.-S. Olesen, and H. Fischer, "Land surface temperature and emissivity estimation from passive sensor data: theory and practice - current trends," *International Journal of Remote Sensing* **23**(13), pp. 2563 – 2594, 2002.
2. A. Berk, L. Bernstein, and D. Robertson, "MODTRAN: A moderate resolution model for LOWTRAN 7.," Tech. Rep. GL-TR-89-0122, Air Force Geophysics Laboratory, Hanscom AFB, MA, 1988.
3. A. Berk *et al.*, "MODTRAN5: A reformulated atmospheric band model with auxiliary species and practical multiple scattering options," in *Algorithms and Technologies for Multispectral, Hyperspectral, and Ultraspectral Imagery X, Proceedings of SPIE, v. 5425*, S. Shen, ed., pp. 341 – 347, 2004.
4. S. Young, B. Johnson, and J. Hackwell, "An in-scene method for atmospheric compensation of thermal hyperspectral data," *J. Geo. Res.* **107**(D24), pp. 14–1 – 14–20, 2002.
5. D. Gu, A. Gillespie, A. Kahle, and F. Palluconi, "Autonomous atmospheric compensation (AAC) of high resolution hyperspectral thermal infrared remote-sensing imagery," *IEEE Trans. Geo. Rem. Sens.* **38**(6), pp. 2257 – 2570, 2000.
6. A. Prata, "Land surface temperatures derived from the advanced very high resolution radiometer and the along-track scanning radiometer 1. theory," *Journal of Geophysical Research* **98**(D9), pp. 16,689 – 16,702, 1993.
7. J. Sobrino, Z.-L. Li, M. Stoll, and F. Becker, "Multi-channel and multi-angle algorithms for estimating sea and land surface temperature with ATSR data," *International Journal of Remote Sensing* **17**, pp. 2089–2114, 1996.
8. Z. Qin, A. Karnieli, and P. Berliner, "A mono-window algorithm for retrieving land surface temperature from landsat tm data and its application to the israel-egypt border," *International Journal of Remote Sensing* **22**(18), pp. 3719 – 3746, 2001.
9. A. Mushkin, L. Balick, and A. Gillespie, "Temperature / emissivity separation of MTI data using the terra/ASTER TES algorithm," in *Algorithms and Technologies for Multispectral, Hyperspectral, and Ultraspectral Imagery VIII, Proceedings of SPIE, v. 4725*, 2002.
10. D. Anding and R. Kauth, "Estimation of sea surface temperature from space," *Remote Sensing of the Environment* **1**, pp. 217–220, 1970.
11. J. Price, "Land surface temperature measurements from the split window channels of the NOAA-7/AVHRR," *Journal of Geophysical Research* **89**, pp. 7231 – 7237, 1984.
12. F. Becker and Z. Li, "Toward a local split window method over land surfaces," *International Journal of Remote Sensing* **11**, pp. 369–393, 1990.
13. J. Sobrino, C. Coll, and V. Caselles, "Atmospheric corrections for land surface temperature using AVHRR channel 4 and 5," *Remote Sensing of the Environment* **38**, pp. 19–34, 1991.
14. Z. Wan and J. Dozier, "A generalized split-window algorithm for retrieving land-surface temperature measurement from space," *IEEE Transactions on Geoscience and Remote Sensing* **34**(4), pp. 892 – 905, 1996.
15. Y. Yu, J. Privette, and A. Pinheiro, "Analysis of the NPOESS VIIRS land surface temperature algorithm using MODIS data," *IEEE Transactions on Geoscience and Remote Sensing* **43**(10), pp. 2340–2350, 2005.
16. J. Schott, S. Brown, R. Raqueño, H. Gross, and G. Robinson, "An advanced synthetic image generation model and its application to multi/hyperspectral algorithm development," *Can. J. Rem. Sen.* **25**(2), pp. 99–111, 1999.
17. E. Ientilucci and S. Brown, "Advances in wide area hyperspectral image simulation," in *Conference on Targets & Backgrounds IX: Characterization and Representation, Proceedings of SPIE, v. 5075*, pp. 110–121, 2003.